Journal of Power Sources 196 (2011) 6412–6418

Contents lists available at ScienceDirect

Journal of Power Sources

journal homepage: www.elsevier.com/locate/jpowsour

Polymer-derived-SiCN ceramic/graphite composite as anode material with enhanced rate capability for lithium ion batteries

M. Graczyk-Zajac*, C. Fasel, R. Riedel

Institut für Materialwissenschaft, Fachgebiet Disperse Feststoffe, Technische Universität Darmstadt, Petersenstr. 23, 64287 Darmstadt, Germany

ARTICLE INFO

Article history:
Received 20 January 2011
Received in revised form 21 March 2011
Accepted 27 March 2011
Available online 5 April 2011

Keywords:
Li-ion batteries
Anode
Graphite
SiCN ceramic

ABSTRACT

We report on a new composite material in view of its application as a negative electrode in lithium-ion batteries. A commercial preceramic polysilazane mixed with graphite in 1:1 weight ratio was transformed into a SiCN/graphite composite material through a pyrolytic polymer-to-ceramic conversion at three different temperatures, namely 950 °C, 1100 °C and 1300 °C. By means of Raman spectroscopy we found successive ordering of carbon clusters into nano-crystalline graphitic regions with increasing pyrolysis temperature. The reversible capacity of about 350 mAh g^{-1} was measured with constant current charging/discharging for the composite prepared at 1300 °C. For comparison pure graphite and pure polysilazane-derived SiCN ceramic were examined as reference materials. During fast charging and discharging the composite material demonstrates enhanced capacity and stability. Charging and discharging in half an hour lead to about 200 and 10 mAh g^{-1}, for the composite annealed at 1300 °C and pure graphite, respectively. A clear dependence between the final material capacity and pyrolysis temperature is found and discussed with respect to possible application in batteries, i.e. practical discharging potential limit. The best results in terms of capacity recovered under 1 V and high rate capability were also obtained for samples synthesized at 1300 °C.

1. Introduction

There is a continuous search for new electrode materials in lithium ion batteries. The development of high energy and high power lithium-ion batteries, in particular in view of commercialization of electric vehicles, is an important technological challenge. Various insertion materials have been proposed as negative electrodes for rechargeable batteries [1–3]. The highest theoretical capacity is obtained when using metallic lithium (3862 mAh g^{-1}) and elemental silicon forming lithium-rich alloys (3578 mAh g^{-1}) [4], however these materials are not commercialized due to safety reasons and rapid capacity fading.

Currently, mostly graphitic materials are used due to low price and high reversibility despite relatively low capacity (372 mAh g^{-1}), instability during long-time cycling and inadequacy for high power applications [5,6]. In consequence, there is still a need for new materials which could be economically interesting but would demonstrate higher capacity, longer life time and better high rate capability. Lithium intercalation into a variety of SiCO and SiCN ceramics derived from various preceramic polymers based on pitch-polysilanes blends [7,8], silanes, siloxanes [9–17] and silazanes [18–23] have been studied during the past 20 years. It was demonstrated that despite the high irreversible capacity analyzed during the first intercalation/extraction, the aforementioned ceramics have to be considered as prospective materials for negative electrodes in lithium ion batteries.

In particular, polymer-derived SiCN ceramics (PDCs) exhibit electrochemical properties suitable for application as electrode material in lithium ion batteries. They are chemically inert with respect to battery components and are lightweight materials. Furthermore, their chemical and physical properties can be designed by varying the starting polymer composition. Various PDCs based on the SiCN and SiCO systems with high carbon content have been reported to exhibit interesting electrochemical properties suitable for the storage of lithium ions [14,15,22,23].

In contrast, low carbon containing SiCN and SiCO ceramics show low Li storage capability insufficient for application as anode material in lithium ion batteries. In particular, within our previous study it was found that pure polyvinylsilazane-derived SiCN ceramic electrodes show a low electrochemical activity, namely a discharge capacity of 35 mAh g^{-1} [18]. However, a composite material comprising the same SiCN ceramic and graphite produced by pyrolysis of a polyvinylsilazane/graphite mixture in the ratio of 75/25 wt% revealed a stable capacity of up to

* Corresponding author.
E-mail address: graczyk@materials.tu-darmstadt.de (M. Graczyk-Zajac).

0378-7753/$ – see front matter © 2011 Elsevier B.V. All rights reserved.
doi:10.1016/j.jpowsour.2011.03.076

600 mAh g^{-1} which significantly exceeds that of pure graphite and SiCN [19,24].

This paper studies the electrochemical performance of a composite anode materials based on commercial graphite (Timcal Ltd., Switzerland) coated with a commercial polysilazane (HTT1800 produced by Clariant GmbH, Germany). The aim of the present investigation is to demonstrate that a SiCN/graphite composite synthesized by pyrolysis of a polyvinylsilazane/graphite mixture in the ratio 1:1 shows significantly enhanced high rate capability as compared to that of pure graphite.

2. Experimental part

2.1. Synthesis of the SiCN/graphite composite

Commercial graphite (SLP50 from Timcal Ltd., Switzerland) and a liquid polyorganosilazane (HTT1800 from Clariant GmBH, Germany) were mixed in 50/50 weight ratio in air to form a slurry at room temperature. The slurry was homogenized for ~10 min by mechanical mixing and was placed in a vertical Heraeus furnace with alumina tube and pyrolyzed under argon atmosphere. The heating rate was about 100 °C h^{-1}, the cooling rate 150 °C h^{-1}. At 230 °C a dwelling time of about 2 h was used in order to further cross-link the polymer. The final temperature (950, 1100 and 1300 °C) was held for 1 h and then the system was allowed to cool down to room temperature.

The preceramic polymer HTT1800 was stored in a glove box (MBraun Glove Box Systems, H_2O/O_2 < 1 ppm) prior to use.

2.2. Preparation of material and electrodes

Prior to electrode preparation each powder was "hand-ground" for 15 min. Carbon black Super P® and SFG6 carbon (both from Timcal Ltd., Switzerland) were added as conducting additives with a ratio of 0.3:9 and 0.6:9 with respect to the composite. Masses of carbon additives (SFG6 and Carbon Black Super P®) were subtracted from the active mass for capacity calculations. The material was mixed with 10% polyvinylidene fluoride (PVdF, SOLEF, Solvay, Germany) solution in N-methyl-2-pyrrolidone (NMP, BASF, Germany). The ratio of carbonaceous material/PVdF was 9:1 and was constant for all the samples. NMP was added in order to form a homogeneous slurry (about 1 g of NMP for 2 g of suspension). The slurry was spread on the rough side of a copper foil (10 μm, Copper SE-Cu58 (C103), Schlenk Metallfolien GmbH & Co. KG, Germany) using a hand blade coating technique and dried at 80 °C for 24 h. The active material loading was always between 6 and 8 mg cm^{-2}. After drying, the circles (electrodes) of 10 mm in diameter were cut. The weight of electrodes was measured, and then the electrodes were dried under vacuum at 90 °C for 48 h in a Buchi oven and transferred directly to the glove box without contact with air.

2.3. Preparation of electrochemical cell

All the electrochemical measurements were performed in two-electrode Swagelok® type cells, with active material as a working electrode and lithium foil (99.9% purity, 0.75 mm thickness, Alfa Aesar, Germany) as a counter/reference electrode. High purity solution of 1 M $LiPF_6$ in ethylene carbonate (EC) and dimethyl carbonate 1:1 of weight ratio (LP30, Merck KGaA, Germany) was used as an electrolyte. A porous polypropylene membrane (Celgard® 2500, Celgard, USA) was used as a separator.

2.4. Characterization techniques

Hermetically closed cells were electrochemically tested by means of galvanostatic and cyclic voltammetry methods using VMP multipotentiostat (BioLogic Science Instruments, France). For galvanostatic charges the cut-off voltages of 0 and 3 V (1.5 V in the case of pure graphite) were used. A constant voltage float was used when the cell reached the cut-off voltage for the slow charging regime (C/20).

In all cases the theoretical capacity of the composite material was assumed to be 360 mAh g^{-1} in order to simplify the comparison with graphite. Accordingly, the following charging/discharging rates, i.e. the following currents have been applied for all investigated materials: C, D/20 = 18 mA g^{-1}, C, D/10 = 36 mA g^{-1}, C, D/5 = 90 mA g^{-1}, C, D/2 = 180 mA g^{-1}, C, D = 360 mA g^{-1}, 2C, 2D = 720 mA g^{-1}. The same rate was used for the charge (C) and for the discharge (D) process.

Micro-Raman spectra were recorded on a confocal micro-Raman spectrometer Horiba HR800 (Horiba, Japan) with an Ar ion laser at a wavelength of 488 nm.

Scanning electron microscopy (SEM) micrographs were obtained using an FEI Quanta600 instrument (FEI, The Netherlands) equipped with an EDX detector with an acceleration voltage of 10–15 kV. Investigated materials were sufficiently conductive so that a vapor deposition of a conductive layer was not applied.

For the chemical analysis of the composites, the carbon content was determined by a carbon analyzer (Leco C-200, Leco Corporation, USA). The oxygen and nitrogen content of the powdered ceramic sample was determined by an N/O analyzer (Leco TC-436, Leco Corporation, USA). The silicon fraction was calculated as the difference to 100% of the sum of the wt%-values of carbon, nitrogen and oxygen, assuming a negligibly small amount of hydrogen in the analyzed samples and no other elements present.

Thermal gravimetric analysis (TGA) measurements were performed using a simultaneous thermal analyzer STA 449C (Netzsch Gerätebau GmbH, Germany) under inert argon gas atmosphere with a flow rate of 25 ml h^{-1} and a heating rate of 5 K min^{-1} in Al_2O_3-crucibles.

3. Results and discussion

3.1. Material characterization: Raman spectroscopy, elemental analysis and SEM investigation

Micro-Raman-spectroscopy was applied to determine the structure of carbon phase in the ceramic samples. We measured the spectra of the composite material as well as of pure HTT1800 thermolysed at similar temperatures. The measured spectra are shown in Fig. 1. The background fluorescence was not subtracted. Fig. 1a presents the Raman spectra obtained from the pure polyorganosilazane HTT1800 heat-treated at 950, 1100 and 1300 °C, while Fig. 1b shows the spectra of the composite materials, C1, C2 and C3 synthesized at 950, 1100 and 1300 °C, respectively and of pure graphite SLP50. The overall relative intensities of the bands related to HTT1800 progressively decreased with increasing pyrolysis temperature. The presented spectra are therefore suitably rescaled for better clarity.

In the spectra there are two significant bands present at 1340 cm^{-1} and 1580 cm^{-1} for all temperatures which correspond to the D and G bands observed in carbonaceous materials [25,26]. The D peak arises from a disorder-induced vibration mode of graphene layers in the carbon phase, linked to the breathing motion of sp^2-rings, while the G mode results from an in-plane bond stretching of sp^2-hybridized carbon atoms [25,27].

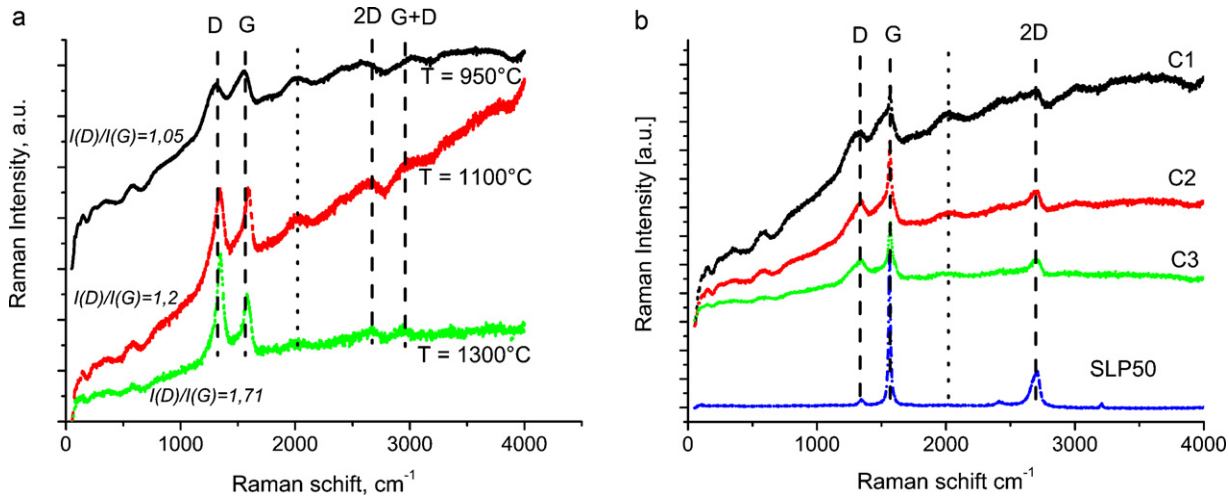

Fig. 1. Raman spectra of pure HTT1800 pyrolyzed at T = 950, 1100, 1300 °C (a) and of the composites C1, C2 and C3 (prepared at 950, 1100, 1300 °C, respectively). The Raman spectrum of the used graphite SLP50 is shown as reference (b). Laser wavelength: 488 nm.

For the pure HTT1800 material (Fig. 1a) the G and D band are better resolved against lower background with increasing pyrolysis temperature. The intensity ratio I(D) to I(G) are 1,05, 1.20 and 1.71 for 950, 1100 and 1300 °C, respectively. To estimate band intensities the fitted baseline was subtracted from the spectra. The shift of the G-band position with increasing pyrolysis temperature from 1540 to 1600 cm^{-1} is also visible.

The presence of the D band is a characteristic Raman feature of disordered carbons, as well as the presence of the band located at 2000 cm^{-1} (dotted line in Fig. 1a) which is attributed to the presence of linear carbon chains [26]. The intensity of the D band increases with the pyrolysis temperature, with increasing ratio of I(D)/I(G). The presence of the G band indicates that the sample contains sp^2-carbon clusters. It implies, in combination with the presence of the D band that a significant fraction of carbon is bonded as a ring-like structure. According to Ferrari et al. the increase of the intensity ratio I(D)/I(G), the decrease of the D peak width and the shift of G peak position from 1500 to 1600 cm^{-1} correspond to the increase in the ordering of the clusters into aromatic graphene layers. The shift of the G band is in reality the appearance of a D′ band at ~1620 cm^{-1}, which merges in the G peak for the small grains. The D′ presence is also characteristic for nanographitic samples. This feature corresponds well to the "three stage model" described by Ferrari [29], i.e. that the observed evolution takes place during the transformation of amorphous carbon to nanocrystalline carbon [28,29]. Additionally new peaks appear at 2670 and 2970 cm^{-1}, denoted in Fig. 1 as 2D and G + D, respectively. Both correspond to overtones of the above mentioned first order modes. The 2D (also called G′) band corresponds to the overtone of the D band and appears in the second-order Raman spectra of crystalline graphite. Its intensity is an indicator of the degree of organization in the graphene layers. The more intense the band the higher the arrangement of graphene sheets and the order in stacking of the layers along the c-axis. In summary, for pure HTT1800-derived materials there is an evolution of the amorphous, disordered carbon clusters into nano-crystalline graphitic regions with increasing pyrolysis temperature. In contrast, the change of the D band (intensity, width) observed for the composite materials (Fig. 1b) is less significant. There is a visible impact of the graphitic part of the composite on the Raman spectrum demonstrated by a narrow intensive G band and well visible 2D band, even at a lower pyrolysis temperature. Surprisingly, the D band remains unchanged at all pyrolysis temperature. Surprisingly, the evolution of the D band of composite is slower than observed for pure HTT1800 material, but nevertheless its width diminishes indicating the ordering of sixfolds aromatic rings [28]. It might indicate that due to the presence of graphite the thermal evolution of disordered carbon into more organized structures is slightly slowed down. The verification of this hypothesis is currently in progress. The increase of the D′ band at ~1620 cm^{-1} signifies the transformation of amorphous carbon to nanocrystalline one as well. In parallel, the width of the G band diminishes, implying that the order of the carbon increases with increasing pyrolysis temperature. The results of the elemental analysis of pyrolyzed HTT1800 and of that of the composite are shown in Tables 1 and 2, respectively.

Table 1
Composition of pure HTT1800 ceramic prepared at 850, 1100 and 1300 °C. Silicon amount calculated as a difference to 100% assuming that we have less than 1 wt% of H in composition.

Sample	C	O	N	Si
950 °C	17.95	2.04	22.35	57.66
1100 °C	18.80	3.42	21.59	56.19
1300 °C	17.99	3.71	22.23	56.07

The composition of the heat-treated pure HTT1800 remains almost identical at all studied temperatures, whereas the composition of the composite changes with pyrolysis temperature. The oxygen content in both cases is related to the contamination due to sample processing. The starting amount of oxygen in the composite is expected to be higher than in pure HTT1800 due to 10 min mixing of HTT1800 with graphite. Nevertheless it should be pointed out that for the composites the amount of oxygen diminishes to less than 1 wt%, while it remains rather constant at 2–4 wt% for the SiCN ceramic derived from HTT1800.

In Fig. 2, SEM images of SLP50 graphite (a) and of the composite samples, C1 (b), C2 (c) and C3 (d), are presented. The SLP50 graphite consists of "potato-shape" particles, mainly 20–40 μm in diameter. For the composites at low magnification (1500 times) we can notice that the graphite particles were not completely destroyed due to the grinding procedure applied after the pyrolysis process.

Table 2
Composition of the composites C1, C2, C3. Silicon amount calculated as a difference to 100% assuming to have less than 1 wt% of H in the materials.

Sample	C	O	N	Si
C1 950 °C	67.25	6.38	7.17	19.20
C2 1100 °C	67.62	2.94	7.65	20.79
C3 1300 °C	69.50	0.87	8.22	21.41

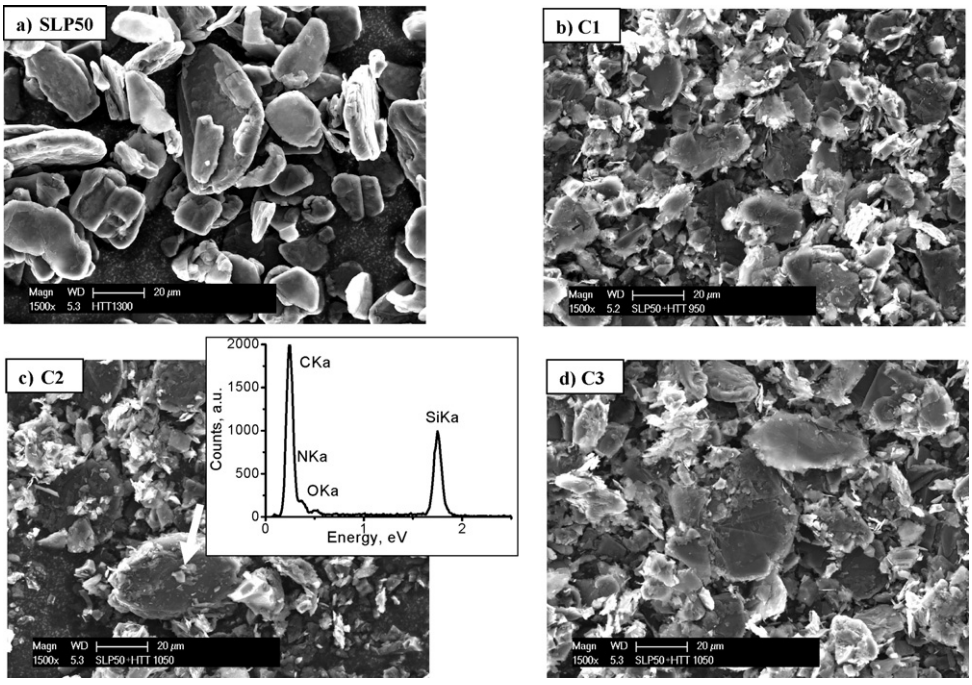

Fig. 2. SEM images of pure graphite (a) and of the composites synthesized at different temperatures (b–d). The inset in (c) represents an EDX analysis of the particle indicated by an arrow.

There is no significant morphological difference between the three composites. Graphitic particles are to be identified and the space in between the C-particles are filled by smaller ones of various sizes <5 μm. In addition, at the surface of some of the graphite particles small grains are found (as indicated with an arrow in Fig. 2c). According to an EDX analysis (see inset in Fig. 2c) the small particles contain silicon and nitrogen in addition to carbon, proving the presence of a SiCN phase.

EDX spectra corresponding to the analysis of selected areas of the microstructure of sample C3 as shown in Fig. 3a are presented in Fig. 3b. A comparable distribution of silicon, carbon and nitrogen was analyzed for C1 and C2 composites. Spectrum 1 presents the elemental distribution of the whole area shown in the micrograph in Fig. 3a. The amount of carbon in the composite material is relatively high in comparison to the amount of carbon measured in pure HTT (Fig. 3b, inset). Nevertheless, the presence of peaks related to silicon and nitrogen unambiguously indicates the formation of SiCN ceramic in between the graphite particles. Small grains of irregular shape as indicated by circles 2 and 3 in Fig. 3a mainly consist of SiCN ceramic.

3.2. Electrochemical studies: first lithium intercalation/extraction cycle

Fig. 4 presents the first galvanostatic insertion/extraction cycle into graphite and composites synthesized at 950 °C (C1), 1100 °C (C2) and 1300 °C (C3). Capacity values obtained during the first charge/discharge and the corresponding capacity losses, i.e. irreversible capacity, are summarized in Table 3. The efficiency, η, is calculated as the ratio of the first discharge (extraction) capacity to the first charge (intercalation) capacity, $C_{rev}/C_{charge} \times 100\%$. This value is considered to be a kind of reference which allows us to estimate the quantity of the irreversible charge loss associated with the first cycle.

Comparing the capacity values from Fig. 4 and Table 3, graphite demonstrates the highest reversible capacity and the best first cycle efficiency with 90% of initial capacity recovered. Sample C1 shows very high first charge capacity (520 mAh g^{-1}), but the value

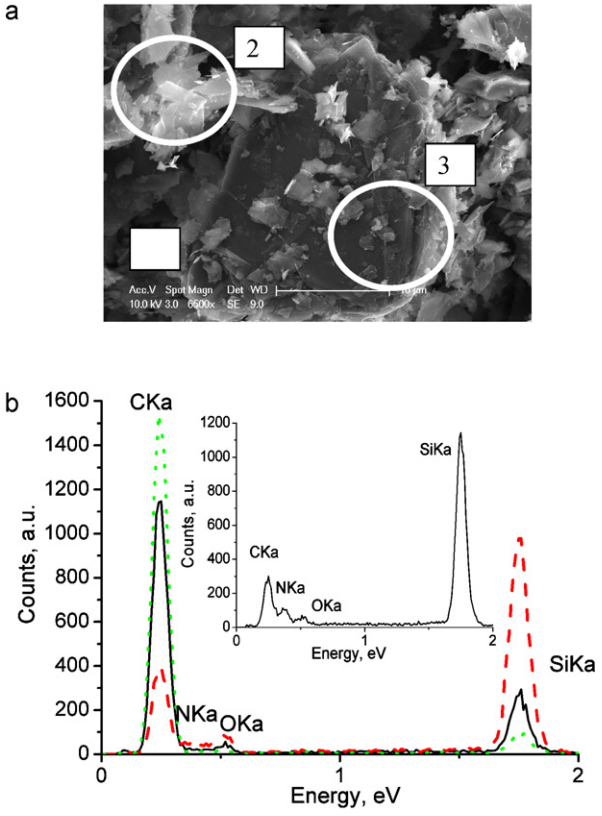

Fig. 3. SEM image of composite C3 (a), and EDX analysis of the whole area shown in (a) (spectrum 1, solid line) as well as that of selected areas indicated by circles, spectra 2 (dashed line) and 3 (dotted line) (b). The inset represents the EDX spectrum of pure HTT pyrolyzed and annealed at 1300 °C.

is recovered only by 72% during the first discharge. Sample C2 demonstrates a somewhat lower irreversibility (133 mAh, η = 74%). The highest reversibility of 76% is registered for sample C3 with a recovered reversible capacity of 312 mAh g^{-1}.

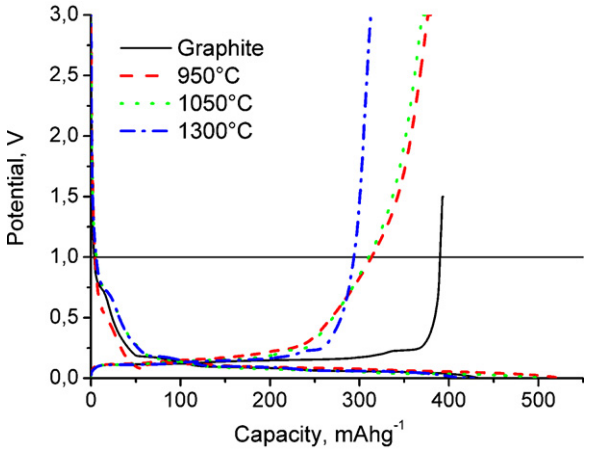

Fig. 4. First lithium intercalation/extraction cycle for pure graphite electrode in comparison with the SiCN/graphite composites prepared at 950, 1100 and 1300 °C.

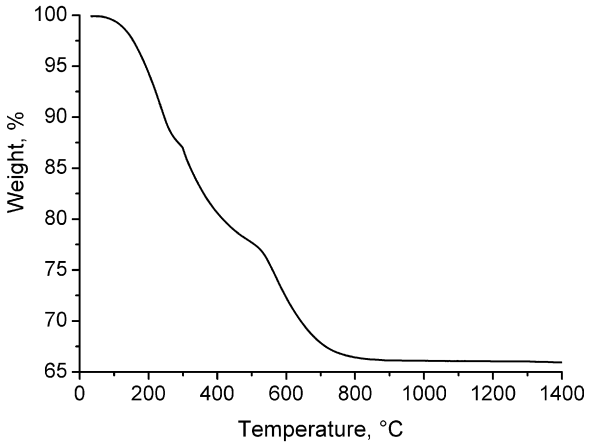

Fig. 5. TGA characteristic of pure HTT1800 polymer.

Note that in Table 3 the values of the reversible capacity and efficiency obtained using the potential limit of 3 V are compared with values of capacity recovered if the potential is limited to 1 V. The lower discharge potential limit is an important factor for the future materials application in lithium ion batteries. When composites discharge up to 1 V, the difference in reversible capacity diminishes significantly while the efficiency of C1 and C2 become much lower. For C3 only slight diminution is found, as shown in Fig. 4, because the major part of the capacity is recovered at the potentials lower than 1 V. This property of sample C3 is an interesting feature for applications in complete batteries where low discharge potential limits are required.

Charging/discharging transients of the samples C1 and C2 differ from the others. The charging curve registered for C1 demonstrates smaller losses related to SEI formation in comparison with C2, C3 and graphite. In contrast, losses registered for C2 and C3 are higher in comparison with graphite. This finding is probably related to the higher active surface of graphite covered by ceramic particles. The discharging part of samples C1 and C2 demonstrates a hysteresis, i.e. that a significant part of the charge is recovered between 0.5 and 3 V. This behavior is typical for disordered carbons synthesized at temperatures below 1100 °C [7,9,11,30,31]. This feature is more pronounced for sample C1, due to the lower thermolysis temperature resulting in a higher amount of disordered carbon. The hysteresis of sample C3 is much less pronounced and the major part of the charge is recovered at a potential below 1 V. The hysteresis increases in the row: graphite < C3 < C2 < C1. According to our knowledge, this kind of electrochemical behavior has not been found neither for SiCN materials synthesized from polysilazanes [21] nor for SiOC ceramics derived from polysiloxanes [32]. Moreover, for siloxane-based materials, an increase of the first charge and discharge capacity is reported with increasing pyrolysis temperature between 900 and 1100 °C. For the materials pyrolyzed at the temperature higher than 1100 °C a significant decrease of capacity is registered. In the case of the SiCN/graphite composites studied in this work, only the first charge capacity follows the tendency found for SiOC ceramics prepared from polysiloxanes [14,21], while the reversible capacity increases slightly with increasing annealing temperature.

The studied composites consist of a considerable amount of graphite which yields a relatively stable capacity. The starting 1:1 ratio of polysilazane HTT1800 to graphite changes during pyrolysis due to mass losses related to the thermal transformation of the preceramic polymer (Fig. 5). Almost 35 wt% of the initial HTT1800 polymer mass is lost during pyrolysis up to $T = 1400$ °C. Therefore, the final material consists of only 40 wt% of SiCN ceramic and 60 wt% of graphite whose mass is assumed to remain stable during thermal treatment. Nevertheless, the 60 wt% of graphite results in a reversible capacity of 230 mAh g^{-1}, while the reversible capacity of the composite amounts to more than 300 mAh g^{-1}. The electrochemical activity of pure SiCN derived from HTT1800 prepared at 1300 °C is shown in Fig. 6. With 10 wt% of conductive additives (6% of SFG6, 4% carbon black) the electroactivity of these additives can be analyzed. If measured without additives, no electroactivity is found although the SiCN phase contains ca. 20 wt% of free carbon (Fig. 6, inset). This behavior is explained by a poor electronic conductivity of the SiCN phase.

Table 3
First cycle charging/discharging capacity, irreversible capacity and coulombic efficiency η of sample C1, C2, C3 and graphite (data from Fig. 4). Efficiency calculated as $C_{rev}/C_{charge} \times 100\%$, $C_{irr} = C_{charge} - C_{discharge}$.

Sample	C_{charge} (mAh g^{-1})	C_{rev} (mAh g^{-1})		C_{irr} (mAh g^{-1})	η (%)	
		3 V[b]	1 V[b]		3 V[b]	1 V[b]
C1 950 °C	520	376	315	144	72	60
C2 1100 °C	507	374	310	133	74	61
C3 1300 °C	412	312	293	100	76	71
Graphite	434[a]	392	390	39	90	90

[a] Presented values are higher than theoretical graphite capacity because for calculations conducting additives were not included in the active mass.
[b] Positive limits of potential for galvanostatic discharging.

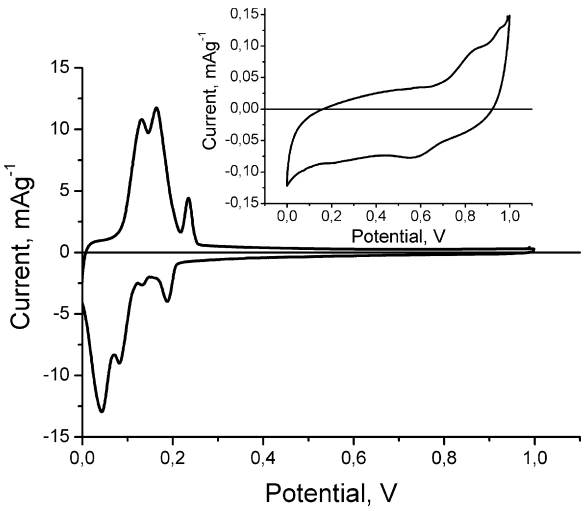

Fig. 6. CV measured for pure SiCN electrode derived from HTT1800 pyrolyzed at $T = 1300$ °C, inset shows the electroactivity of the SiCN electrode without conductive additives. Scan rate 10 μV s^{-1}.

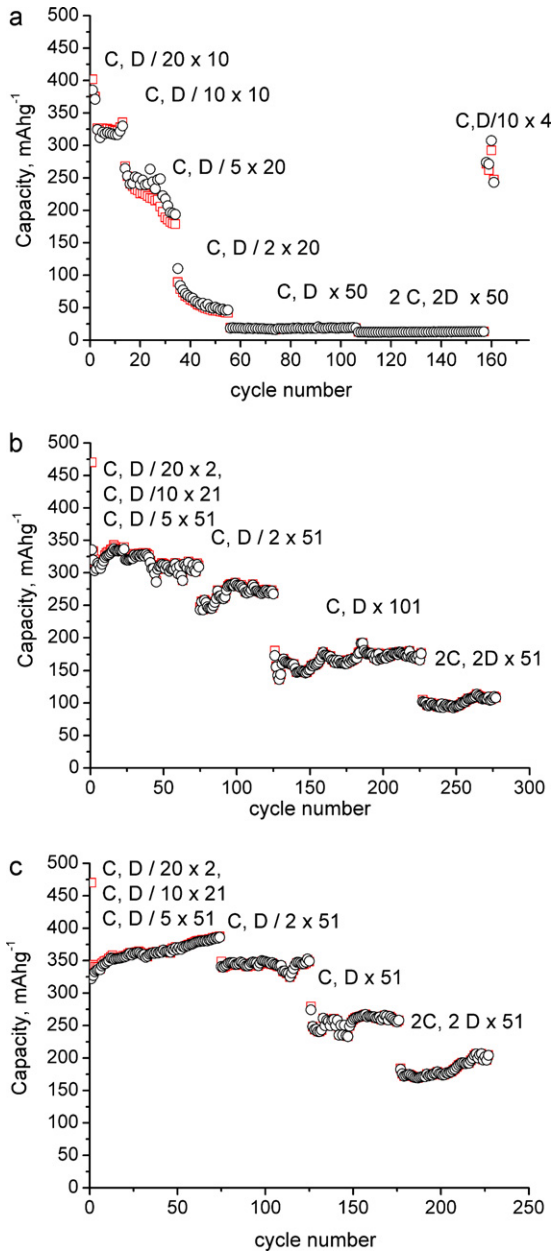

Fig. 7. Extended cycling behavior (capacity vs. cycle number) of graphite electrode (a) and composite electrode prepared at 1100 °C (b) and 1300 °C (c). C, D rates are indicated in figure.

We believe that the SiCN ceramic can deliver the capacity only in the presence of an excess of well conductive support, e.g. graphite. In that case, the support supplies the paths for electronic contact and the charge can be transmitted to the SiCN phase. In consequence, mixing the SiCN ceramic with graphite provides electronic contact between the ceramic particles which are well dispersed in the graphitic matrix (Fig. 2) and the capacity of the ceramic can be fully exploited.

3.3. Extended-cycling electrochemical behavior

Fig. 7 shows the extended cycling behavior of pure graphite, as well as that of the composites C2 and C3 (Fig. 7a–c, respectively). Since samples C1 and C2 represent similar electrochemical behavior for extended cycling only C2 is demonstrated here. The pure graphite sample (7a) exhibits a stable behavior only for low charge/discharge rates (C, D/20, C, D/10). The capacity diminishes significantly, namely from 330 mAh g^{-1} recovered for C, D/10 to 175 mAh g^{-1} after 20 cycles, when the charging rate increases up to C, D/5. Further diminution is analyzed for C, D/2. With higher rates the negligible amount of capacity is recovered. It is known that graphite is able to be discharged with very high rates, up to 10C, if subsequently charged with lower current. However, the inverse procedure gives different results, i.e. graphite reveals a poor charge capability, even if faster charge is followed by slow discharge [33]. It has been found that from the thermodynamic point of view for any lithium ion intercalating electrode, the extraction process should be more favorable than the intercalation one, because the lithium ions acquire higher mobility [34].

However, if charge and discharge are performed at the same rate, the performance of graphite is affected noticeably. Recently, it has been discussed by Sivakkumar et al. [35] that SLP50 graphite (and other graphitic materials) shows rapid fade of capacity with increasing CD rate. The fading rate increases with increasing electrode thickness. Sivakkumar presented in his study that less than 20% of initial capacity was recovered at 2C, 2D rate, and less than 5% with higher currents for the thickest studied electrode (100 μm). Note that in the present study we used electrodes of 6–8 mg cm^{-2} of active materials, i.e. 2.5–3.7 mAh cm^{-2}, so the thickness of electrodes varied from 160 to 220 μm (both for graphite and composites). Therefore, the values presented in Fig. 7a, are in agreement with previous literature investigations even though they appear surprisingly low.

In contrast to the behavior of graphite, the electrochemical stability of the SiCN/graphite composite versus lithium intercalation/extraction is significantly enhanced for higher currents (Fig. 7b and c). It should be kept in mind that the electrode loading and thickness of the composite materials were similar to that of graphite. For the composite prepared at 1100 °C (and similar for the C1 composite) the recovered capacity is almost not affected by the increase of the current, up to a rate of C, D/5. With increasing rate the recovered capacity diminishes to ~250 mAh g^{-1}, ~150 mAh g^{-1} and ~100 mAh g^{-1} for C, D/2, C, D and 2C, 2D, respectively. The values remain stable even during extended cycling (i.e. 100 cycles at the C, D rate). The results found for the composite C3 (Fig. 7c) are even more pronounced in this aspect. During cycling, the capacity increases and the increase of the C, D rate has no influence on it. When the material is charged at a rate of C, D/2 the recovered capacity diminishes only slightly. At a C, D rate of 2C and 2D a capacity of about 250 mAh g^{-1} and almost 200 mAh g^{-1} is recovered, respectively.

In order to explain this phenomenon, we take into account the results described in the first part of this work related to the morphological characterization of the composites. We discussed that graphite particles are surrounded by a ceramic layer, consisting of carbon, silicon and nitrogen. During the first charge process a passivation layer (*Solid Electrolyte Interface* (SEI)) is formed on the surface of the graphite particles. This process is responsible for an irreversible capacity loss, but also serves as a protection against co-intercalation of solvent molecules resulting in graphite exfoliation [1,36]. The formation of a stable SEI stabilizes the graphite surface and allows only non-solvated lithium ions to pass through and to intercalate inside the graphite lattice [6]. It has been postulated that it is highly probable that the limiting step of the lithium diffusion is associated with the SEI layer, its interfaces as well as with the electrolyte–SEI interlayer [35]. To diffuse through the SEI the lithium ion must de-solvate, requiring energy to diffuse across the SEI. In the case of our SiCN/graphite composite, the SEI is not formed directly on the graphite particles (assuming that graphite particles are completely covered by SiCN), but on the ceramic layer. The results of our present study indicate that the faster transport of lithium ions with the result of higher recovered charge /discharge

capacities is related to the presence of this SiCN layer. Thus, the ceramic part not only adds some capacity to the system, but it also provides a particular stability to the graphite grains for faster insertion/extraction of lithium ions.

Furthermore, we assume that the capacity increase found during cycling (in particular for slower charging rates) for the composite C3 is due to a structural reorganization of the composite material during lithium intercalation/extraction. As a result, new conducting paths are formed resulting in higher capacity values.

4. Conclusion

In this article we present the investigation of a new composite material consisting of graphite and SiCN ceramic as anode material for lithium ion batteries. In terms of lithium ion insertion/extraction, the composite exhibits a higher capacity than that of the sum of both components. Raman experiments demonstrate that an increase of the pyrolysis temperature increases the order of the carbonaceous part for pure SiCN derived from the commercial polysilazane HTT1800. In contrast, in the presence of graphite the thermal evolution of disordered carbon into higher organized derivatives seems to be slowed down. An electron microscopic investigation reveals that in the case of the composite materials, the SiCN ceramic is uniformly distributed among graphite particles. Our findings clearly indicate that the remarkably stable capacity of the composite, in particular when synthesized at 1300 °C, is due to the presence of the SiCN ceramic phase. The outstanding electrochemical properties of the SiCN/graphite composites are related to the presence of the well conducting (electron and Li ion conduction) graphite matrix. Graphite supplies the paths for electronic contact and thus the charge can be transmitted to the disordered carbons formed within the polymer-derived SiCN phase.

Moreover, due to their particular morphology (graphite surrounded by SiCN ceramic particles) and composition, the new composites reveal extraordinary stability during high current charging/discharging processes. The composites synthesized at 1300 °C recover the major part of the capacity under 1 V, underlining the enormous technological potential of the novel composite anode material. In conclusion, SiCN ceramic/graphite composites are interesting “high power” anode materials for various applications of Li-ion batteries such as portable power suppliers and electric vehicles.

Acknowledgments

We gratefully acknowledge the financial support by the Deutsche Forschungsgemeinschaft (DFG), Bonn, Germany (SFB 595/A4). Thanks to Timcal Pty. Ltd. for supplying graphite material.

MG-Z thanks PD Dr. Helmut Ehrenberg for fruitful scientific discussion, Miria Andrade for her help with Raman experiments and George Bedenian for his help in electrode preparation. R.R thanks the Fonds der Chemischen Industrie, Frankfurt, Germany for financial support.

References

[1] M. Winter, J.O. Besenhard, M.E. Spahr, P. Novák, Adv. Mater. 10 (1998) 725–763.
[2] P. Bruce, B. Scrosati, J.-M. Tarascon, Angew. Chem. Int. Ed. 47 (2008) 2930–2946.
[3] U. Kasavajjula, C. Wang, A.J. Appleby, J. Power Sources 163 (2007) 1003–1039.
[4] M.N. Obrovac, L. Christensen, Electrochem. Solid State Lett. 7 (2004) A93–A96.
[5] N. Takami, A. Satoh, M. Hara, T. Ohsaki, J. Electrochem. Soc. 142 (1995) 2564.
[6] J.O. Besenhard, M. Winter, J. Yang, W. Biberacher, J. Power Sources 54 (1995) 228.
[7] W. Xing, A.M. Wilson, G. Zank, J.R. Dahn, Solid State Ionics 93 (1997) 239–244.
[8] J.R. Dahn, A.M. Wilson, W. Xing, G.A. Zank, inventors; Dow Corning Corp., assignee, Method of forming electrodes for lithium ion batteries using polycarbosilanes, United States Patent US 5907899, 1999, June 1.
[9] H. Fukui, H. Ohsuka, T. Hino, K. Kanamura, ACS Appl. Mater. Interface 2 (2010) 998–1008.
[10] W. Xing, A.M. Wilson, K. Eguchi, G. Zank, J.R. Dahn, J. Electrochem. Soc. 144 (1997) 2410–2416.
[11] A.M. Wilson, G. Zank, K. Eguchi, W. Xing, J.R. Dahn, J. Power Sources 68 (1997) 195–200.
[12] J.R. Dahn, A.M. Wilson, W. Xing, G.A. Zank, inventors; Dow Corning Corp., assignee, Electrodes for lithium ion batteries using polysilanes, United States Patent US 6306541 (B1), 2001, October 23.
[13] J.R. Dahn, K. Eguchi, A.M. Wilson, W. Xing, G.A. Zank, inventors; Dow Corning Corp., assignee, Electrodes for lithium ion batteries using polysiloxanes, United States Patent US 5824280(A). 1998 October 20.
[14] D. Ahn, R. Raj, J. Power Sources 196 (2011) 2179–2186.
[15] J. Shen, D. Ahn, R. Raj, J. Power Sources (2010), doi:10.1016/j.jpowsour.2010.11.009.
[16] P.E Sanchez-Jimenez, R. Raj, J. Am. Ceram. Soc. 93 (2010) 1127–1135.
[17] D. Ahn, R. Raj, J. Power Sources 195 (2010) 3900–3906.
[18] R. Kolb, C. Fasel, V. Liebau-Kunzmann, R. Riedel, J. Eur. Ceram. Soc. 26 (2006) 3903–3908.
[19] M. Graczyk-Zajac, C. Fasel, G. Cherkashihnin, W. Jaegermann, R. Riedel, LiBD-4 2009 – Electrode materials. Arcachon, France 20-25 September 2009, Novel graphite/SiCN negative electrode materials for lithium-ion batteries with enhanced capacity and rate capability, extended Abstract.
[20] J.R. Dahn, A.M. Wilson, W. Xing, G.A. Zank, inventors; Dow Corning Corp., assignee, Electrodes for lithium ion batteries using polysilazanes ceramic with lithium, United States Patent US 5631106(A), 1997, May 20.
[21] D. Su, Y.-L. Li, Y. Feng, J. Jin, J. Am. Ceram. Soc. 92 (2009) 2962–2968.
[22] M. Graczyk-Zajac, G. Mera, J. Kaspar, R. Riedel, J. Eur. Ceram. Soc. 30 (2010) 3235–3243.
[23] J. Kaspar, G. Mera, A. Nowak, M. Graczyk-Zajac, R. Riedel, Electrochim. Acta 56 (2010) 174–182.
[24] M. Graczyk-Zajac, C. Fasel, R. Riedel, Unpublished results.
[25] F. Tuinstra, J.L. Koenig, J. Chem. Phys. 53 (1970) 1126–1130.
[26] A.C. Ferrari, J. Robertson, Phys. Rev. B 64 (2001) 075414.
[27] M.A. Pimenta, G. Dresselhaus, M.S. Dresselhaus, L.G. Canc, A. Jorio, R. Saito, Phys. Chem. Chem. Phys. 9 (2007) 1276–1291.
[28] N. Janakiraman, F. Aldinger, J. Eur. Ceram. Soc. 29 (2009) 163–173.
[29] A.C. Ferrari, J. Robertson, Phys. Rev. B 61 (2000) 14095–14107.
[30] J.R. Dahn, T. Zheng, Y. Liu, J.S. Xue, Science 270 (1995) 590–593.
[31] M. Jean, C. Desnoyer, A. Tranchant, R. Messina, J. Electrochem. Soc. 142 (1995) 2122–2125.
[32] A.M. Wilson, J.N. Reimers, E.W. Fuller, J.R. Dahn, Solid State Ionics 74 (1994) 249–254.
[33] H. Buqa, D. Goers, M. Holzapfel, M.E. Spahr, P. Novak, J. Electrochem. Soc. 152 (2005) A474–A481.
[34] H. Shi, J. Power Sources 75 (1998) 64–72.
[35] S.R. Sivakkumar, J.Y. Nerkar, A.G. Pandolfo, Electrochim. Acta 55 (2010) 3330–3335.
[36] K. Guerin, A. Fevrier-Bouvier, S. Flandrois, M. Couzi, B. Simon, P. Biensan, J. Electrochem. Soc. 146 (1999) 3660–3665.